Experimental and numerical study of the fuel effect on flame propagation in long open tubes

Guillaume Lecocq, Jérôme Daubech, Emmanuel Leprette

Experimental and numerical study of the fuel effect on flame propagation in long open tubes

Guillaume Lecocq [a], Jérôme Daubech [a] & Emmanuel Leprette [a]

Institut National de l'Environnement Industriel et des Risques, Parc Technologique ALATA, BP 2, 60550 Verneuil-en-Halatte, France

E-mail: guillaume.lecocq@ineris.fr

Abstract

Previous works (Daubech, Lecocq, 2019) were dedicated to gaseous flame acceleration along long pipes with a set of cases studied both experimentally and numerically. In these cases, the flammable mixture was initially quiescent and homogenously distributed. The impact of the tube diameter and material were studied trough both approaches for rather slow flames, the fuel being methane. While main features of the real flame were recovered by the chosen CFD method, some limits remained.

A new experimental dataset is detailed and analyzed with a quicker flame, the fuel being hydrogen and the same experimental set-up as the one used for measuring slow flames. Thus, the fuel effect on the flame dynamics can be directly highlighted.

A simple CFD approach is tested for recovering two distinct flame behaviors: a deflagration flame and another undergoing deflagration-to-detonation transition. Furthermore, the modelling results are used to propose elements of interpretation for flame acceleration.

Keywords: *premixed gaseous flame propagation, hydrogen, methane, pipes, CFD*

1. Introduction

Scenarios of formation of gaseous flammable clouds in long ducts can be identified during risk analyses of industrial processes. If an ignition occurs, a flame can propagate in such flammable cloud and undergo an acceleration which is specific to this confined and elongated geometry.

If the flammable cloud formation and the ignition cannot be avoided, it is key to assess the flame acceleration process and the generated pressure effects associated to the explosion scenario. These latter should be compared to the mechanical resistance properties of the pipe in which the explosion could be triggered. To do so, the flame acceleration process has to be understood with the specificities of the explosion scenario (tube material and diameter, flammable cloud length, spatial distribution of the fuel in this cloud, …).

Previous experimental and numerical works were detailed for 24 m long pipes made of PMMA or steel, with varying diameters (150 or 250 mm), the fuel being methane (Daubech, Lecocq, 2019). The pipes were open at one end and closed at the other where ignition was triggered. The tests showed the impact of the pipe material and diameter.

In the current work, new experimental data are presented. They correspond to the case of a 150 mm wide steel tube in which a homogenous hydrogen/air cloud with a volume fraction of 20 % is ignited. They are compared to another experimental point for which the flammable cloud is made of a stochiometric methane/air cloud.

A CFD approach is proposed and tested, in order to assess its predictive capacities and study if elements could be extracted from computations for helping to interpret experiments.

2. Experimental set-up and results

The current work is dedicated to flames propagating in a straight, 24-m long steel pipe, open at one end and closed at the other. Ignition is performed on the middle of the closed end with an electrical spark whose energy is about 100 mJ.

Two initially quiescent flammable mixtures are studied:

- A stoichiometric methane/air mixture,
- A lean hydrogen/air mixture, with a hydrogen volume fraction in air of 20 %.

Figure 1 shows the pipe in which flame propagation is measured.

Fig. 1. *View of the experimental set-up. Steel pipe, with a 150-mm inner diameter.*

The flame position is tracked with four photovoltaic cells located at 0.5 m, 5.5 m (4.5 m for methane), 10.5 m and 15.5 m from ignition point. Pressure signals are measured with three probes close to ignition point and at 5 m and 15.5 m from ignition point. The acquisition bandwidth is 15 kHz for the methane flame and 20 kHz for the hydrogen one. More details about the experimental set-up are given of the paper of Daubech (2019).

The two experiments described in the paper belong to a large database which was produced in the framework of the EXPRO project. The aim of the experimental campaign was to investigate the effect of numerous parameters such as the tube diameter, its material (steel or PMMA), the equivalence ratio of the flammable mixture, the effect of singularities (elbows, restrictions) on the flame dynamics. A limited number of sensors for pressure and flame position was sufficient for this parametric study. It should be added that for all conditions of the database, two tests were performed. A good repeatability was encountered.

Raw experimental results for the reacting front trajectory and pressure signals are given in Figures 2-3 and Figures 6-7 for both fuels. Two different behaviors can be noticed.

For the methane/air flame, while the flame front speed keeps on increasing, its maximum value remains about 140 m/s. Two main peaks can be seen for each pressure signal.

The first one can be explained with flame elongation that follows ignition, which leads to an increase of the burnt gases volume variation per time unit. When this variation becomes weaker, because a maximum in flame surface is reached, the pressure decays. The flame continues to accelerate,

eventually with a change in flame shape, and the volume production of burnt gases creates the second peak which is limited by the amount of flammable mixture in the tube. A maximum overpressure about 400 mbar is reached. The time needed to burn all the flammable mixture is between 0.25 s and 0.3 s.

For the hydrogen/air case also, a continuous acceleration of the flame front can be noticed. A maximum speed higher than 2000 m/s is measured for the reacting front. This value can be compared to the Chapman-Jouguet velocity, about 1710 m/s. In this case, a transition from a deflagration regime to a detonation one (DDT) is observed.

At the pressure probe located 5.5 m away from ignition point, a first peak similar to the first peak identified for the methane/air flame appears. A slight pressure decay then occurs and is followed by a continuous pressure increase until a maximum overpressure of 3 bar. 15.5 m away from ignition point, a shock wave appears with a peak about 20 bar. This value is higher than the Chapman-Jouguet pressure (13 bar), which, additionally to what was said for the reacting front velocity, indicates an overdriven detonation.

3. Phenomenology related to explosions in pipes and CFD modelling

3.1 Phenomenology

Cicarelli et al. (2008) proposed a review article dedicated to flame acceleration in pipes. With ignition, a burnt gases kernel is created, which leads to the formation of a premixed laminar flame. It is first wrinkled due to Darrieus-Landau instability, which is promoted or counteracted by thermo-diffusive effects, respectively if the Lewis number is lower or higher than 1. In the same time, the fresh gases are pushed ahead of the flame front due to thermal expansion effects. The flame front then reaches the lateral wall of the tube, leading to slight deceleration of the burnt gases production, the flame surface being reduced. It can be also promoted by heat losses, depending on the tube material. This initial sequence of flame propagation leads to the production of a set of pressure waves that set into motions the fresh gases ahead of the flame. The flame keeps on propagating with a shape that can sequentially change from an elongated flame to a tulip-shape flame, still pushing the fresh gases. The flame acceleration mechanism in this phase remains discussed.

With his pioneer works, Shchelkin (1940, 1965) explained flame self-acceleration in tubes with flame/turbulence interaction, turbulence being produced in the fresh gases after generation of a boundary layer on the walls. This explanation highlights the importance of the wall roughness on the flame dynamics. Experiments (Daubech, 2019) carried out for methane/air flames propagating in long open tubes with different materials (ie PMMA for a smooth tube and steel for a rough tube) led to different flame dynamics provided the tube diameter was small enough. Indeed, no significant change was observed for a 250 mm-wide tube while a 150 mm-wide tube led to a more dynamic flame when the material was steel. The same set of experiments also showed the wall turbulence remained limited at the walls for the widest tubes while flame acceleration was noticed. The theoretical work of Deshaies and Joulin (1989) notably studied the compressive heating of the fresh gases, related to the propagation of a precursor shock wave ahead of the flame front. According to them, while these compressive effects tend to accelerate the flame, they do “not always imply an every accelerating flame”. They also showed the flame folding, generated according to them by turbulence, was of importance for the history of flame dynamics. If a critical flame folding could be reached for a sufficiently long time along with the heating effects mentioned above, then the flame could accelerate limitlessly.

According to Cicarelli et al. (2008), a detonation can be first initiated after a shock reflection or a shock focusing. The shock is strong enough to auto-ignite fresh gases and trigger detonation. This mechanism is encountered in closed and/or obstructed tubes. In unobstructed tubes, the most probable mechanisms are more subtle ones involving instabilities and mixing processes. These phenomena

were first explained by Zeldovitch (1970) and Lee (1978) with the formation of an induction time gradient, due to local inhomogeneities (temperature and/or concentration). The related spontaneous flame would release heat and create a shock wave. If the heat release strengthens the shock wave sufficiently, a detonation can occur. Another work (Ivanov, 2011) called into question this mechanism. According to the authors, DDT could occur when the reacting front is so fast that formed shock waves sit on this latter and a coupling mechanism leads to a sufficient increase of the reacting front speed and pressure peak. A similar result was proposed by Clavin and Tofaili (2021) trough modeling. DDT was also explained in a recent work (Melguizo-Gavilanes, 2022) coupling experimental results and modeling by a late flame acceleration, generating a secondary precursor shock, stronger than the first one.

3.2 Modelling approaches available in the literature

CFD approaches available in the literature for flame acceleration in tubes rely either on a highly detailed description of the flow (Oran, 2007) or "under resolved" modelling that are built with numerous sub-models, each one accounting for a physical feature (Wieland, 2021).

Such models often rely on a progress variable ($\tilde{c}$). This quantity evolves monotonically and is normalized, its value ranging between 0 and 1. The first value corresponds to a fresh gases state, the second to the burnt gases state. The flame front is then localized with the gradient of the progress variable. The chemical source term which pilots the propagation speed of the flame front can be simply closed as the product of this gradient, the density of the fresh gases (ρ^u) and a characteristic flame front speed: $\bar{\rho}\,\widetilde{\omega_c} = \rho^u S_F|\nabla\tilde{c}|$. The flame speed $S_F$then writes: $\Xi.S_L$ where Ξ is a wrinkling factor. This latter is explained as the product of characteristic wrinkling factors, each one accounting for a phenomenon accelerating the flame speed: thermo-diffusive and Darrieus-Landau instabilities, pressure effects, …

Some authors (Wieland, 2021, Bradley, 2012) describe detonation as the coupling of auto-ignition of fresh gases coupled to the propagation of a shock wave. Chemical source terms can be built from two contributions (Lecocq, 2011, Wieland, 2021): one modelling a premixed flame, the other auto-ignition, in order to account for the transition between the deflagration and the detonation.

3.3 Approach retained

The computations presented in the current work are based on a modelling strategy close to the one of Wieland (2021) for modelling deflagrations. The transport equations are solved for momentum, pressure, a progress variable and energy with a pressure-based solver of the CFD code OpenFoam v2106 (Weller, 1998). Turbulence is also modelled with a k-ω SST model (Menter, 2003).

Concerning the methane/air flame the pressure effects remain moderate. A constant laminar flame speed of 0.4 m/s was used. The pressure effects are well higher for the hydrogen/air flame and they have to be included for the estimation of the fresh gases density ρ^u and the laminar flame speed S_L. ρ^u is simply quantified under the assumption of an adiabatic compression, thanks to the pressure field. Correlations can be found in the literature for the laminar flame speed of hydrogen, these latter accounting for a dependance with initial pressure and temperature. The high dependance of the hydrogen laminar flame speed on the fresh gases temperature is highlighted by numerous resources (Bane, 2010, Bougrine, 2011). Nevertheless, it is not clear according to the bibliography if the hydrogen laminar flame speed should increase or decrease with pressure, when confronting detailed chemistry computations (Bane, 2010, Bougrine, 2011) and some experimental data (Salzano, 2012). It should be noted that according to Bane (2010), the dependance of the hydrogen flame speed on fresh gases temperature is much more pronounced than the dependance on pressure. For the present computations, for the sake of simplicity, a constant laminar flame speed value of 0.9 m/s is used for the hydrogen flame.

The wrinkling factor Ξ is closed as: $\Xi = \Xi_t . \Xi_I$ where Ξ_t represent flame wrinkling induced by flame/turbulence interaction and is closed with the turbulent flame speed correlation proposed by Gülder (1991). The wrinkling factor Ξ_I represents the effects of instabilities. The commonly made assumption of a unitary Lewis number for methane/air flames is kept and Ξ_I is set to 1.0 in this case. Concerning the hydrogen/air flame, its Lewis number, about 0.5 (Bauwens, 2012), is smaller than 1.0 and instabilities at the flame front are expected. A value for Ξ_I remains hard to predict. An ad hoc way was to tune it in order to recover a proper reacting front trajectory with time. A constant value of 3.35 was identified. There is no model for auto-ignition in the retained approach.

The computational domain is limited to the part of the pipe filled by the flammable mixture. At walls, velocity is zero and turbulent viscosity is modelled with a wall law. At the outlet plane, the pressure is set to the atmospheric pressure and the velocity gradient is set to 0.

The walls are assumed to be adiabatic (temperature gradient set to 0). The steel roughness is assumed to be around 150 μm which corresponds to a weakly rusted steel. This characteristic is used in the wall laws.

The 3-D mesh is made of 2.5 million hexahedra, with 36 cells in the tube diameter. The maximum characteristic cell width is about 6 mm. The time derivative is discretized with a first order (Euler) scheme while second orders schemes are used for the convection and diffusion operators. There was no specific procedure for capturing the shocks.

4. Results

4.1 Case of the methane flame

According to Figure 2, the computation enabled to recover a qualitative agreement for the evolution of the flame front position with time. The increase in flame velocity is satisfying from t = 0 s to t = 0.05 s and from t = 0.15 s to t = 0.25 s but is overpredicted from t = 0.05 s to t = 0.15 s.

Figure 3 shows the main features of the pressure signals are predicted. At 5.5 m and 10.5 m, there is a first pressure peak, followed by a pressure decay and one or several peaks. The amplitude of the first pressure peak is about 200 mbar and the second is about 400 mbar. The overestimation of the first peak by the modelling is about 25 % while the second one ranges from 25 to 50 %.

It should be here noted that the results depend on the mesh as finer cells lead to a delayed flame acceleration corresponding to an underpredicted secondary pressure peak.

It is interesting to go a little bit further in the computation post-processing as several quantities can explain pressure effects. Indeed, these latter are related to the volume rate at which burnt gases are produced by flame propagation, the tube acoustics and the effect of the opening.

Using a method previously used in a LES context (Richard, 2007), the total flame surface density contained in a cell can be seen as the product of:

- the ‘sub-grid’ wrinkling factor that represents the amount of flame distortion not solved by the mesh (the factor Ξ),
- the gradient of $\tilde{c}$ which represents the local amount of flame surface per cell volume solved by the mesh (*ie* local solved flame surface divided by the local cell volume).

The total flame surface captured by the mesh is quantified as: $S_{res} = \int_V |\nabla \tilde{c}| \, dV$. A resolved wrinkling, Ξ_{res}, can be defined as the ratio of this surface to the tube section. The turbulent wrinkling averaged on the flame surface, $< \Xi_t >_s$ is also computed. The evolution of these quantities with time is plotted in Figure 4.

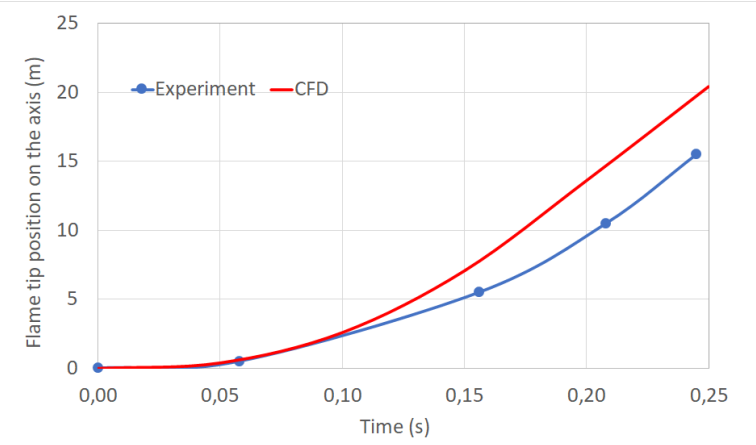

Fig. 2. Experimental and computed flame trajectory on the axis for the methane/air flame.

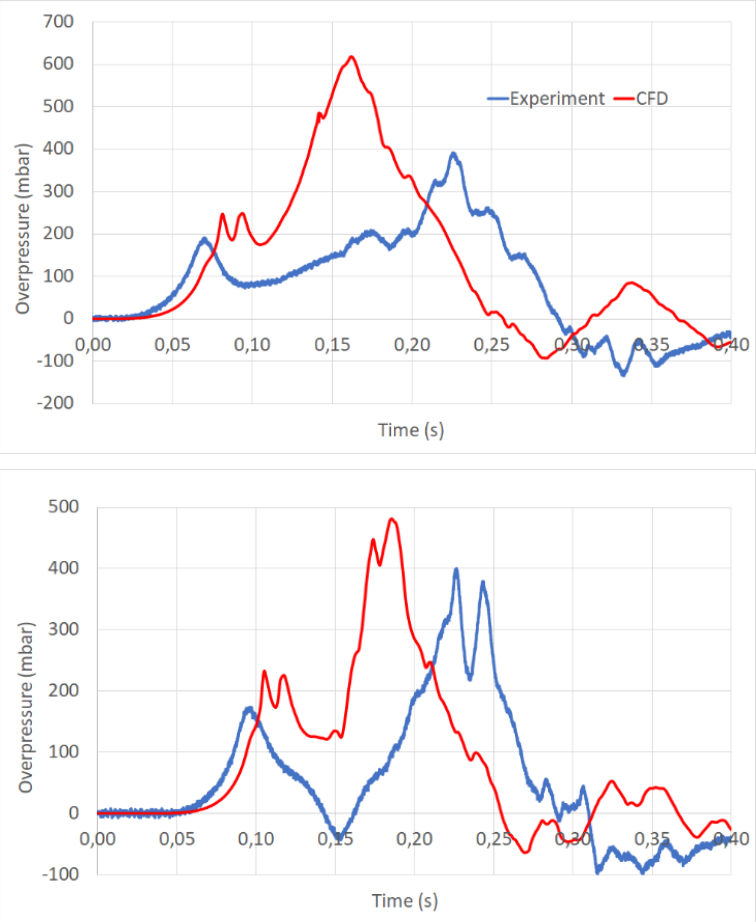

Fig. 3. Experimental and computed pressure signals at 5.5 m (top) and 15.5 m (bottom) from ignition point for the methane/air flame.

$< \Xi_t >_s$ mainly increases with time, starting from t = 0.05 s. The final value reached is about 15. Ξ_{res} does not follow the same evolution: there are two cycles of increase/decrease and a constant value is observed for the final propagation phase. The maximum value is about 8. According to the

Figure 5, the maximum values, reached for example at t = 0.05 s and t = 0.15 s correspond to elongated flames. The lowest values at the end of flame propagation are obtained for quasi-flat flames.

It is notably interesting to note that:

- the first pressure peak at 0.07 s seems to be mainly explained by flame elongation and very weak flame/turbulence interaction,
- the pressure decay that follows is related to the change of the flame shape (from an elongated shape to a tulip shape),
- the pressure peak at 0.15 s is obtained when the product $< \Xi_t >_s . \Xi_{res}$ is the highest.

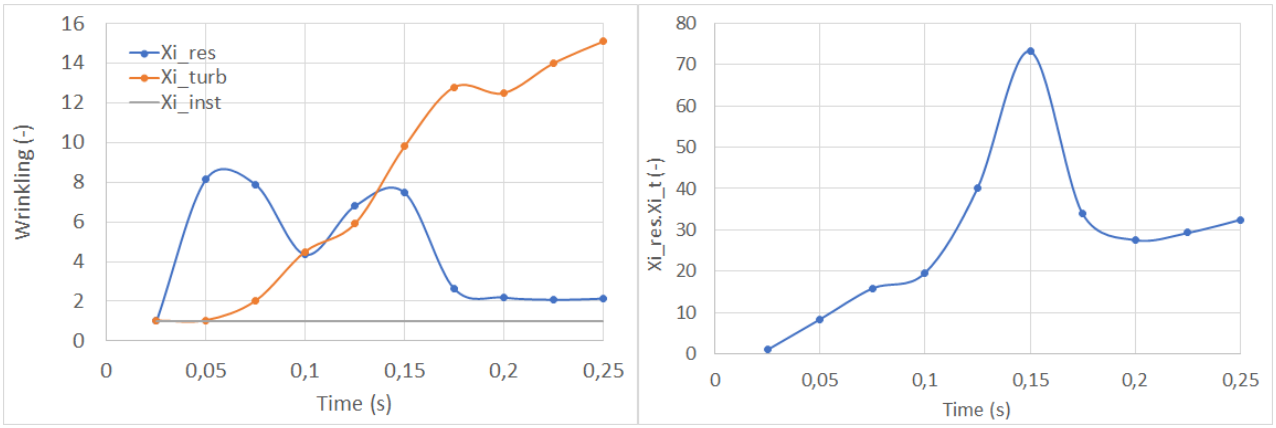

Fig. 4. Time evolution of the characteristic wrinkling factors (left) and of the product of all wrinkling factors (right) of the methane/air flame.

The effect of flame dynamics can be seen on the pressure field for several instants in Figure 6. At 50 ms, the pressure is the highest behind the flame front and progressively decays towards the atmospheric pressure. Between 50 and 100 ms, the structure of the pressure field changed: two pressure waves were emitted, they are respectively located at 5 and 10 m from the flame front. Their magnitudes correspond to the pressure peaks in the tube at 100 ms. At 150 ms, due to the significant flame acceleration between 100 and 150 ms, the pressure reaches its peak value just ahead of the flame front and decays towards the atmospheric pressure. A pressure wave is emitted between 150 and 200 ms as the production of burned gases decays with the flame shape change. Between 200 and 250 ms, the pressure keeps on decreasing in the tube.

4.2 Case of the hydrogen flame

Figure 7 shows the experimental and predicted reacting front trajectory for the hydrogen flame. It should be recalled here that the parameter Ξ_I was adjusted to recover a satisfying reacting front trajectory.

Figure 8 highlights the main trends of the pressure signals were recovered. At 5.5 m, the computed pressure signal is characterized with three peaks, with an overall pressure increase. The amplitude of the pressure is closed to the measured one. 15.5 m away from ignition point, the measured shock wave is predicted, nevertheless with a peak overestimation of 75 %. This proves a pressure-based solver is able to deal with shocks. Other authors choose to change their solver when the reacting front velocity exceeds a critical value (Wieland, 2021).

As mentioned for the methane flame, the results depend on the mesh as finer cells lead to a delayed DDT and a less good agreement with the experimental flame dynamics.

The characteristic wrinkling factors are also plot for the hydrogen reacting front (Figure 9). $< \Xi_t >_s$ mainly increases, starting from 0.01 s to 0.06 s and then decreases. The peak value is very high (70

ie about 5 times the peak value observed for the methane/air flame). As for the methane/air flame, Ξ_{res} sequentially increases and decreases. The orders of magnitude of the peak values are close to those obtained for the methane/air flame.

The first pressure peak seems to be explained by an increased flame surface as well as flame instabilities. A pressure decay is observed, related to a rapid change of the flame shape which is not compensated by flame instabilities and flame/turbulence interaction. After this phase, while the flame shape and surface evolve (Figure 10), the reacting front acceleration is mainly promoted by turbulence effects, until the end of the reacting front propagation in the tube. It should be noted that the topology shown at t = 65 ms, characterized by a flat shock wave followed by a funnel-shaped flame was notably observed through experiments by other authors at a lower scale quite recently (Ballossier, 2021)

The evolution of the pressure field is shown in Figure 11. At first, a pressure wave is emitted, between t = 10 ms and t = 20 ms. This was also observed with the methane flame. Later, as it can be seen at t = 35 ms, this pressure wave evolved into a shock wave. It propagates well ahead of the flame front. Just after the flame front, there is a pressure wave whose magnitude corresponds to the peak pressure in the tube. At the later instants, this pressure wave progressively turns into a shock wave, always followed by the flame and its magnitude keeps on increasing as well as its propagation speed. It finally catches the preceding shock wave before it goes out of the tube.

Here DDT was approached through a continuous turbulent flame acceleration until the reacting front reaches the preceding shock wave. This point of view is closed to the Shchelkin one but it may be too much simple compared to realistic mechanisms. It is indeed possible that the CFD model should predict flame extinction instead of flame acceleration. Indeed, when a laminar flame undergoes turbulence effects, its response changes according to the turbulence intensity. For sufficiently low turbulence intensity, the flame speed increases with increasing turbulence intensity. When turbulence intensity is high enough, the flame speed increase is weaker ('bending effect') and the flame may extinguish if the turbulence is even higher (Nivarti, 2017). It is expected that DDT is triggered before flame extinction due to the occurrence of other phenomena, notably if pressure and temperature conditions of the fresh gases could locally correspond to an auto-ignition delay lower than the characteristic time of flame propagation. Thus, the employed CFD model should be completed with extinction and auto-ignitions models.

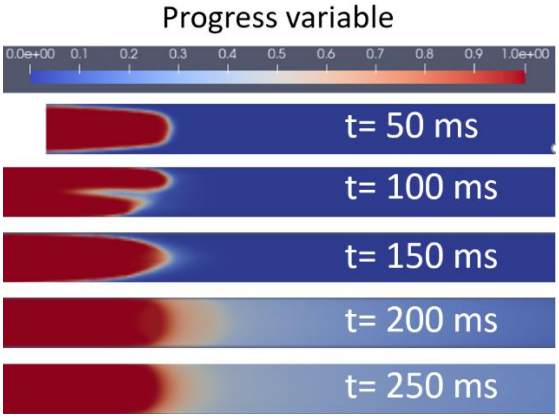

Fig. 5. Evolution with time of the flame shape for the computed methane/air flame.

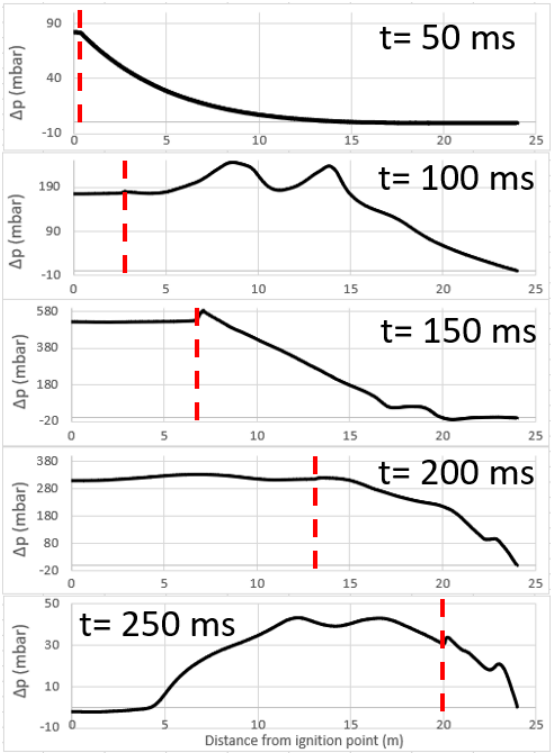

Fig. 6. Evolution with time of the pressure field for the computed methane/air flame. The red dash line corresponds to the flame tip position.

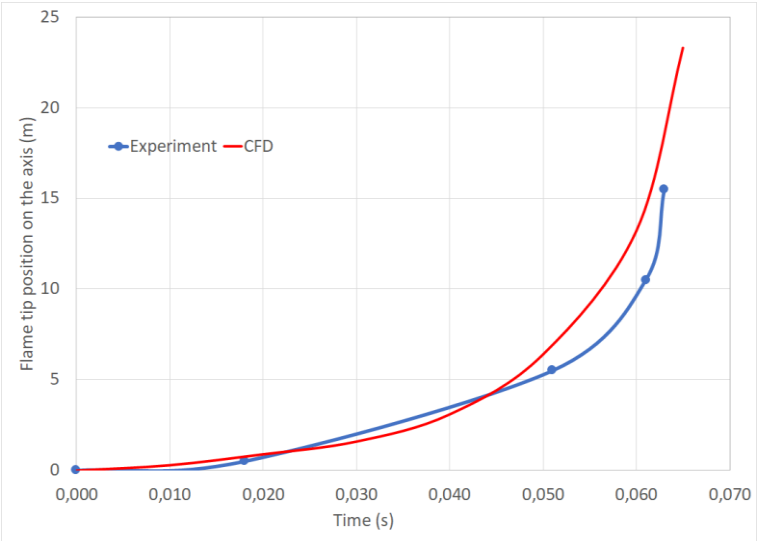

Fig. 7. Experimental and computed reacting front trajectory on the axis for the hydrogen/air flame

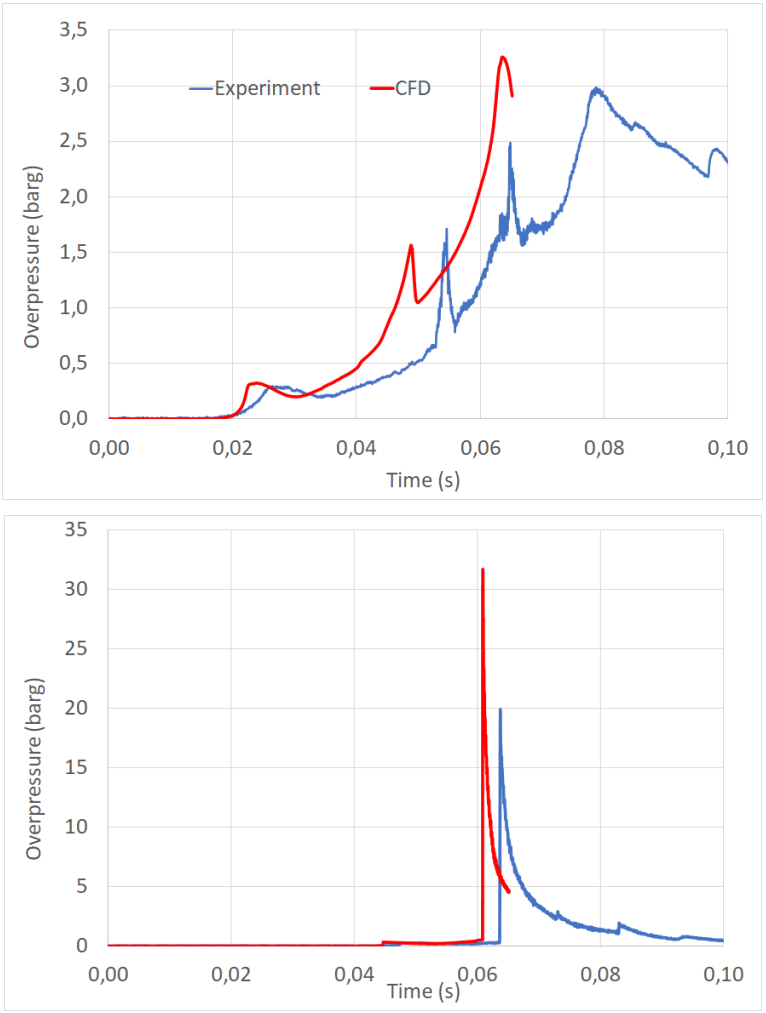

Fig. 8. Experimental and computed pressure signals at 5.5 m (top) and 15.5 m (bottom) from ignition point for the hydrogen/air flame.

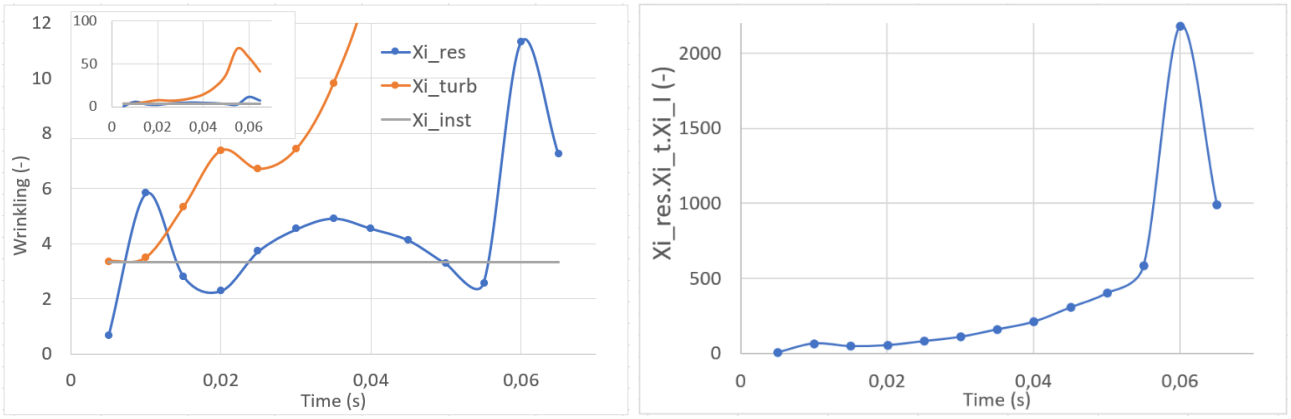

Fig. 9. Time evolution of the characteristic wrinkling factors (left) and of the product of all wrinkling factors (right) of the hydrogen/air flame.

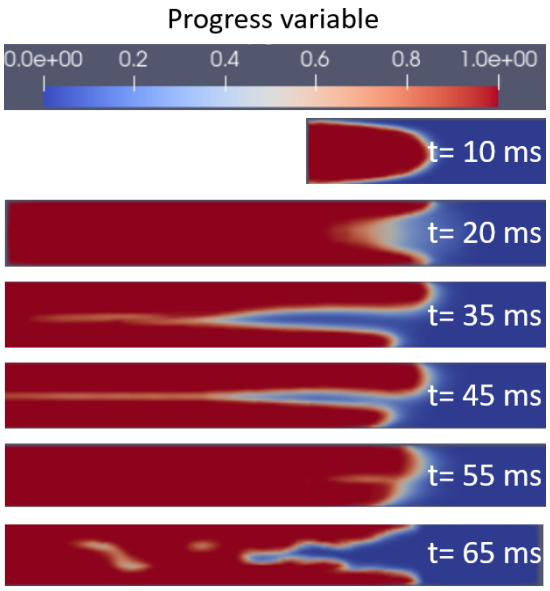

Fig. 10. Evolution with time of the flame shape for the computed hydrogen/air flame.

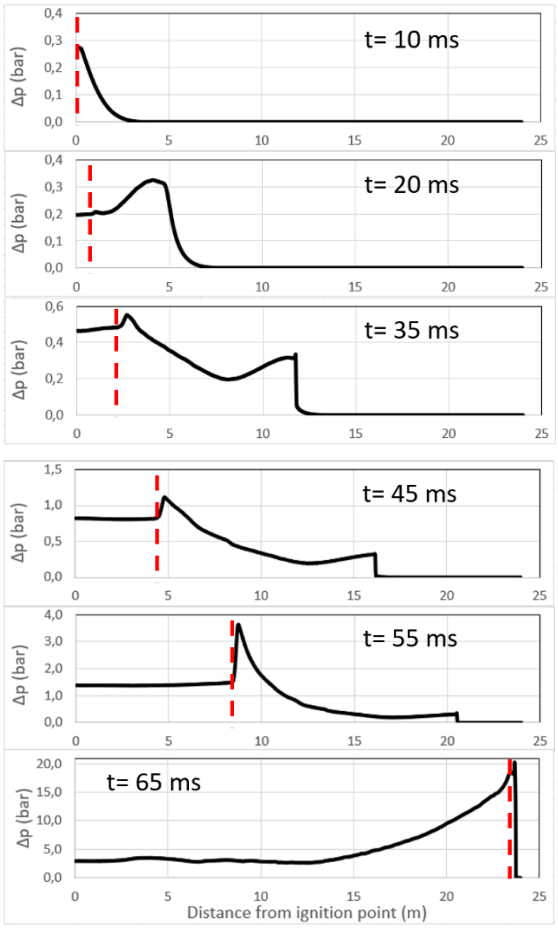

Fig. 11. Evolution with time of the pressure field for the computed hydrogen/air flame. The red dash line corresponds to the flame tip position.

5. Conclusions

Experimental results were first shown for a 24 m long steel pipe in which initially quiescent flammable mixtures were ignited, one being a stoichiometric methane/air mixture, the other a lean hydrogen/air mixture.

Two distinct flame behaviours were observed: the maximum propagation speed of the methane/air flame was about 140 m/s while DDT occurred for the hydrogen/air flame.

A simple CFD model was used to recover features of both cases. An agreement was found for flame position with time and pressure effects.

The raw CFD results were post-processed to give pieces of interpretation for what was observed. One interest of CFD here is to give access to more quantities than the measured ones. Thus, it was possible to study the effect of turbulence, instabilities and flame shape changes on the pressure effects.

Nevertheless, the current CFD model should be completed with other sub-models (extinction, autoignition sub-models, …) as it is possible that the acceleration for the hydrogen flame, numerically explained by flame/turbulence interaction is not as large as predicted.

Acknowledgements
The authors gratefully acknowledge the financial contribution granted by the Research Fund for Coal and Steel (RFCS) for the EXPRO project during which the presented experimental data were produced

References

Daubech, J., Proust, C., Leprette, E., Lecocq, G. (2019). Further insight into the gas flame acceleration mechanisms in pipes. Part I: experimental work. *Journal of Loss Prevention in the Process Industries* 62, 103930

Lecocq, G., Leprette, E., Daubech, J., Proust, C. (2019). Further insight into the gas flame acceleration mechanisms in pipes. Part II: numerical work. *Journal of Loss Prevention in the Process Industries* 62, 103919

Cicarelli G. and Dorofeev S. (2008*)* Flame acceleration and transition to detonation in ducts. *Progress in Energy and Combustion Science* 34, pp. 499-550

Shchelkin KI (1940*)* Influence of the wall roughness on initiation and propagation of detonation in gases. *Zh Eskp Teor Fiz* 10, pp. 823-827.

Shchelkin KI, Troshin YaK (1965*) Gas dynamics of combustion. Baltimore: Mono book corp.*

Deshaies, B., & Joulin, G. (1989). Flame-speed sensitivity to temperature changes and the deflagration-to-detonation transition. *Combustion and flame*, 77(2), 201-212.

Zeldovitch YaB, Librovich VB, Makhiviladze GM. Sivanshinsky GI (1970) On the development of detonation in a non-uniformy preheated gas. *Astronautica Acta* 15, pp. 313-321

Lee JHS, Knystautas R, Yoshikawa N (1978) Photochemical initiation and gaseous detonations. *Acta Astronautic*a 5, pp. 971-972

Clavin, P., & Tofaili, H. (2021). A one-dimensional model for deflagration to detonation transition on the tip of elongated flames in tubes. Combustion and Flame, 232, 111522.

Melguizo-Gavilanes, J. & Bauwens, J. (2022). An experimentally informed 1-D DDT model for smooth narrow channels. 28th International Colloquim on the Dynamics of Explosions and Reactive Systems. Napoli, ITA

Ivanov M.F., Kiverin A.D., Liberman M.A. (2011) Flame acceleration and DDT of hydrogen-oxygen gaseous mixtures in channels with no-slip walls. *Int. J. of Hydrogen Energy* 36, pp. 7714-7727

Lecocq G., Richard S., Michel J.-B., Vervisch L. A new LES model coupling flame surface density and tabulated kinetics approaches to investigate knock and pre-ignition in piston engines, *Proceedings of the Combustion Institute* 33(2) (2011) 3105-3114

Oran E.S., Gamezo E.N. (2007) Origins of the deflagration-to-detonation transition in gas-phase combustion. *Combust. Flame* 148, pp. 4-47

Wieland C., Scharf F., Shildberg H.-P., Hoferichter V., Eble J., Hirsch C., Sattelmayer T. (2021) Efficient simulation of flame acceleration and deflagration-to-detonation transition in smooth pipes. *Journal of Loss Prevention in the Process Industries* 71, 104504

Bradley D (2012) Autoignitions and detonations in engines and ducts, *Phil. Trans. R. Soc. A* (2012) 370, 689–714

Weller, H.G, Tabor, G. (1998). A tensorial approach to computational continuum mechanics using object-oriented techniques. *Computational Physics*, 12: 620-631.

Menter F.R., Kuntz M., and Langtry R. (2003). Ten years of industrial experience with the SST turbulence model. *Proceedings of the international symposium on turbulence, heat and mass transfer*, 4: 625–632.

Gülder O. (1991*)* Turbulent premixed flame propagation models for different combustion regimes. *Proc. Combust. Inst. 23, pp. 743-750*

C.R. Bauwens et al. (2012) Effect of hydrogen concentration on vented explosion overpressures from lean hydrogen/air deflagrations, *Int. Journal of Hydrogen Energy* 37: 17599-17605

S. Richard et al. (2007), Towards large eddy simulation of combustion in spark ignition engines. *Proc. Combust. Inst.*, 31: 3059–3066

Bane, S. P. M., Ziegler, J. L., Shepherd, J. E. (2010). Development of one-step chemistry models for flame and ignition simulation. GALCIT Report GALTCITFM, 2010, 53.

Bougrine S. et al. (2011) Numerical study of laminar flame properties of diluted methane-hydrogen-air flames at high pressure and temperature using detailed chemistry. *Int. Journal of Hydrogen Energy* 36, pp 12035-12047

Salzano E. et al. (2012) Explosion behavior of hydrogen-methane/air mixtures. *J. Loss Prev. In the Process Ind.* 25, pp. 443-447

G. Nivarti et al. (2017) Direct Numerical Simulation of the bending effect in turbulent premixed flames, *Proc. Combust. Inst.* 36:1903-1910

Ballossier, Y., Virot, F., Melguizo-Gavilanes, J. (2021). Strange wave formation and detonation onset in narrow channels. Journal of Loss Prevention in the Process Industries, 72, 104535